ASSESSMENT OF HYPERION FOR CHARACTERIZING MANGROVE COMMUNITIES

Martina Demuro and Laurie Chisholm[1]

1 Introduction

Mapping the distribution of species and vegetation types in coastal wetlands has become important because of the need for wetland inventories and their biodiversity (Finlayson *et al.,* 1999; Phinn and Finlayson, 1999). Vegetation is also regarded as a bio-indicator of site conditions and it is therefore important to understand changes in its distribution and the process acting upon it (Küchler, 1988; Blasco *et al*., 1996; Muller, 1997; Klemas, 2001). Mapping methods need to be efficient and cost effective (Mumby *et al*., 1999) with satellite remote sensing systems having been used extensively for mapping the distribution of vegetation types in coastal wetlands and other environments (Gross *et al*., 1989; Phinn *et al*., 1999). The detection of vegetation types will depend directly on the sampling unit used by the sensor (pixel) and the area imaged. The signal recorded for each pixel is composed of a mixture of components that characterize each community, including the species, canopy openness, height and substrate. Broad-band multispectral imagery is usually analyzed using methods that classify whole pixels using limited spectral information (Vane and Goetz, 1993), which do not account for the problem of mixed pixels. The discrimination of vegetation types using satellite-borne sensors is usually based on the structure (height, openness) and broad vegetation categories (such as woody, perennial, evergreen) (Lewis, 1999; Holmgren and Thuresson, 1998). A common criticism of satellite remote sensing is its inability to define features of interest that are related to ecological processes because of the crude spectral and spatial dimensions of the images (Rougharden *et al.,* 1991; Holmgren and Thuresson, 1998). Advantages of higher spectral resolution imagery include the acquisition of detailed spectral information of the features on the ground (Ustin *et al.,* 1991) and the possibility of image analysis procedures that aim to detect target spectra at a sub-pixel level (Curran, 1994; Clark, 1999; Mustard and Sunshine, 1999). Airborne hyperspectral data have been used to detect minerals and plant biochemicals that have distinct absorption features (Curran, 1994; Serrano *et al.,* 2002) and species distribution (Dehaan and Taylor, 2002; Parker Williams and Hunt Jr., 2002). EO-1 Hyperion is the first satellite-borne hyperspectral sensor to orbit the Earth, capable of recording spectral information superior to previous satellite sensors. Hyperion differs from previous satellite sensors in that it records radiance in many narrow contiguous bands spanning the visible to the near infrared portion of the spectrum. Hyperion has a spatial resolution of 30 meters and records radiance in 220 bands spanning from the blue at 450 nm to the middle infrared at 2500 nm. Each band has a width of approximately 10 nm.

1.1 Objectives

This study aims to assess Hyperion for its ability to discriminate vegetation types based on species composition. The study focuses on the vegetation of coastal wetlands, namely temperate mangrove, saltmarsh and casuarinas forests. To the authors' knowledge there are currently no studies that have tried Hyperion imagery for mapping mangrove species diversity and saltmarsh vegetation as yet.

2 Study Site

The study was conducted in the Minnamurra River estuary, New South Wales. The study area is located approximately between S 34˚ 36' and 34˚37' and between E 150˚50' and E 150˚51'. The estuary sub-catchment area where this study is based is approximately 10 km^2 (Figure 2.1). The estuary is in an advanced stage of infilling and the river follows a meandering channel characterized by three bends flowing around three sand deposits (Carne, 1991). The Minnamurra River estuary has been listed as a nationally important wetland in Australia because "it is a good example of a wetland type occurring within a biogeographic region in Australia" and because "the wetland supports native plant or animal taxa or communities which are considered endangered or vulnerable at the national level" (Environment Australia 2001).

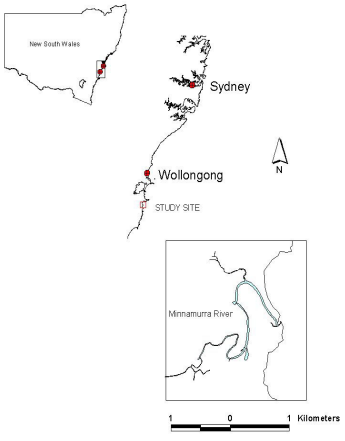

Figure 2.1. **S**tudy site location in NSW, Australia.

[1] School of Geosciences, University of Wollongong (laurie_chisholm@uow.edu.au)

2.1 Vegetation

The estuarine vegetation of the Minnamurra estuary has been described in a number of studies (Carne, 1991; Chafer, 1997). The vegetation in the muddy intertidal zone is composed of mangroves and saltmarsh (Figure 2.2). A swamp-oak forest composed of casuarina trees extends to the landward side of the mangrove and saltmarsh vegetation, outside the tidal range (Chafer, 1997). A littoral forest is found further inland, which has a patchy distribution. The widths of the mangrove, saltmarsh and swamp oak forest areas are usually smaller than 500 meters. Other cover types surrounding the estuary include: to the east, an extensive residential area, to the north a waste disposal depot and some artificial water bodies, and to the west, at higher elevations, an area composed of grasslands.

Two mangrove communities have been identified in the temperate mangroves of Australia (Saenger *et al.,* 1977). These are the *A. marina* low closed-forest and *A. marina* low woodland. The *A. marina* low closed-forest is a monospecific stand of *A. marina* trees that have a foliage cover of over 70 % and a height of less than 10 m. The *A. marina* woodland is composed of both *A. marina* trees and *A. corniculatum* shrubs. The term woodland corresponds to areas where the projective foliage cover of the upper stratum (*A. marina*) is very low (10-30 %) and the trees have a height of less than 10 m. A mid-stratum of both the shrub *A. corniculatum* and a 'dwarf' variation of *A. marina* become very extensive in this community. Similar to other temperate mangroves of New South Wales, the distribution of each community in the Minnamurra estuary is characterized by the formation of low closed-forests in the low intertidal zone, especially at the mouth of the estuary, while the low woodland develops to the landward side of the monospecific *Avicennia marina* forests (Carne, 1991).

Saltmarsh communities develop to the landward side of the mangroves, with the succulent *Sarcocornia quinqueflora* dominant in the low marsh area, while the grass *Sporobolus virginicus* and the rush *Juncus kraussii* dominate in the middle marsh areas. The reed *Phragmites australis* becomes dominant in less saline areas of the saltmarsh. Swamp-oak forests develop to the landward side of the mangrove and saltmarsh vegetation exclusively composed of the *Casuarina* spp. trees that grow extensively at higher elevations in Minnamurra.

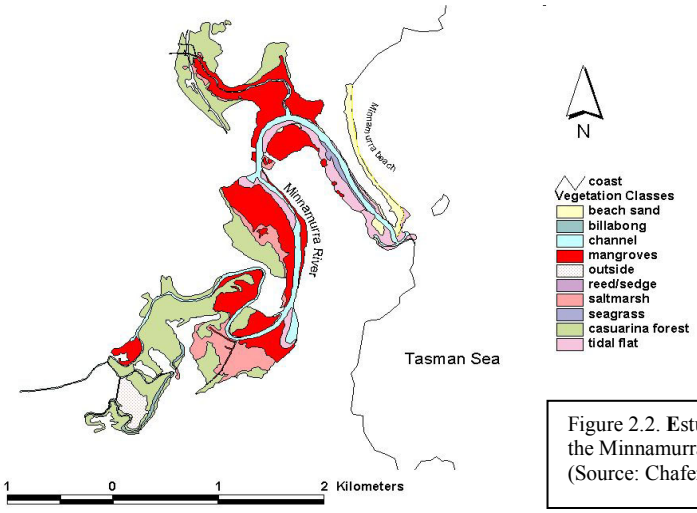

Figure 2.2. **E**stuarine vegetation of the Minnamurra River Estuary. (Source: Chafer, 1997)

3 Methods

3.1 Field data collection

Eleven plots of 90 m × 90 m each (3×3 pixels) were taped in the field: two of *Avicennia marina* low closed-forest, three of *A. marina* low woodland, five of the saltmarsh vegetation and two of the casuarina forest. The plots were made facing north in order to ensure that the largest number of pixels possible covered the plots. The tape and compass method was used to tape the plots. Each corner was marked using 1.5 m high stack marked with flagging tape. A Trimble ProXL GPS with TDCI data logger was used to obtain the coordinates of each corner. The points were verified to correspond to each corner by plotting these over a geo-referenced aerial photograph and deciding if

these coincided with each known point in the field. The coordinates of each corner were displayed in Arcview GIS and it was confirmed that the plots were rectangular and positioned in a south-north direction.

The information collected for mangroves included, for each plot, the projective foliage cover of the upper and mid-stratum, average height and the relative abundance of *A. marina* and *A. corniculatum*. The projective foliage cover was estimated using the gap-ratio method (McDonald *et al*., 1984) and the relative abundance of each species was estimated using the line-intercept method. In the saltmarsh, the relative abundance of each species was measured for each plot. In the casuarina forest, the canopy closure and height of trees was sampled and an average calculated in order to determine the structural heterogeneity of the forest in each plot.

3.1.1 Structure and floristic of vegetation in each plot

The *A. marina* low closed-forest was composed of 100% *Avicennia marina* trees of an average height from 4 to 5.7 m in both plots. The projective foliage cover was approximately 50% in each plot and the gap between the crowns was 12 cm, while average crown diameter was from 250 to 1000 cm in each plot, indicating high canopy closure. The *A. marina* low woodland was composed of both A. marina and *A. corniculatum* species. In the low woodland vegetation, the relative abundance (aerial cover) of each species was over 50% for *A. corniculatum* and less than 30% for *A. marina*. The upper-stratum was dominated by isolated *A. marina* trees with a projective foliage cover of less than 10% and a mean gap between crowns of more than 7 m. The mid-stratum was dominated by *A. corniculatum* shrubs in all sites, with a projective foliage cover of approximately 40% in all sites. The saltmarsh vegetation was divided into low-marsh, dominated predominantly by the succulent herb *Sarcocornia quinqueflora* and the grass *Sporobolus virginicus*, and the mid/upper-stratum, dominated by *Junkus kraussii*, *Phragmites australis* and *Sporobolus virginicus*. The casuarina forest plots were composed of 100% *Casuarina* spp. trees, with both plots having the homogeneous forest formations.

3.2 Satellite hyperspectral imagery acquisition and characteristics

The EO-1 Hyperion image was acquired by USGS (United States Geological Survey)/EROS Data Center, Sioux Falls, South Dakota, USA, on 27 July 2002 at about 10:30 a.m. (local time). The Hyperion data consist of a data 'cube' represented by 242 spectral bands acquired over an array of 256 pixels (width). The number of lines (length) varies with the data acquisition event and the image is built up with the forward motion of the sensor (Jupp *et al.*, 2002). The image acquired over the study area was 7.7 km wide and 185 km long.

3.3 Pre-processing

3.3.1 Atmospheric and geometric correction

All pre-processing and analysis of the EO-1 Hyperion imagery was done using the image processing system ENVI® (Environment for Visualizing Images, Research Systems, Inc.). The EO-1 Hyperion image was atmospherically corrected in order to convert the data from at-sensor-radiance to apparent reflectance. The "coastal Waters and Ocean MODTRAN-4 Based ATmospheric correction" (c-Wombat-c) implemented in IDL/ENVI® was used. The c-WOMBAT-c applies a full MODTRAN-4 atmosphere parameterization and characterization to run the inversion from radiance to reflectance. The parameters correspond to very dry and clear atmospheric conditions without aerosol contents. An inspection of a false color composite agreed with these parameters since the image appeared very contrasted and without hazy effects. A spatial subset of 4 km wide by 5.7 km long was selected from the image to define the Minnamurra estuary study site, including the upland areas and coastal waters. The image was geometrically corrected using an image-to-image registration procedure using an ortho-rectified georeferenced aerial photograph of the area as reference. The image was registered to the Australian Map Grid 66 (AMG) coordinate system using 6 control points obtained from the photograph. A polynomial nearest-neighbor algorithm was applied. In this method, the pixel that has its center closer to the point located in the image is transferred to the corresponding display grid location (Richard and Jia, 1999). This technique does not alter pixel brightness values. The average RMS was 0.259 or within 1 pixel. Vegetation and cadastral vector files of the area were overlaid to observe the correspondence between the image and the geo-referenced files. After inspecting a number of points it was concluded that the registration was satisfactory.

3.3.2 Band selection

Of the 242 bands only 198 are calibrated to radiance while the rest are set to zero (Jupp *et al.*, 2002). The 198 bands were viewed through the animation tool in order to select noise-free bands for further processing. Bands

corresponding to water absorption features were very noisy containing no spatial information and were subsequently excluded from the data set. Streaking was apparent in some bands from both the VNIR and SWIR regions. Streaking is presented as vertical lines related to the along-track effects of push-broom systems (Jupp *et al.,* 2002) and are more apparent in low SNR (signal to noise ratio) bands. The streaking effect was pronounced in the SWIR region, specifically between 2000 nm and 2500 nm. De-streaking was initially attempted, however, the resulting images appeared worse than the originals. Consequently only bands 207 and 208 were retained from the 200-2500 nm region. All other bands deemed to have unacceptable noise or streaking were also removed. In total 105 bands were selected for further use.

3.4 Image analysis

3.4.1 Mixture Tuned Matched Filtering (MTMF)

The *Mixture Tuned Matched Filtering*™ (MTMF) is a technique that works by partially unmixing pixel spectra according to a user-defined endmember. In this procedure, the response of the reference endmember spectra is matched to the pixel spectra by maximizing the endmember response and masking the background unknown response (ENVI, 2001). The results indicate the degree to which the endmember was matched to the pixel spectra and the approximate sub-pixel response of the endmember (ENVI, 2001). An image is produced where bright pixels indicate high abundance of the endmember and therefore a high MF (matched filtering) score. An infeasibility result is also produced that represents the 'false positives' and assigns high infeasibility scores values to pixels erroneously matched to the endmember (see ENVI 2001 for details). This approach has been used to determine biochemical composition of leaves using data sets of leaf spectral response (Pinzon *et al.,* 1998) and species discrimination in saltmarsh vegetation (Zhang *et al.,* 1996) and the discrimination of a weed species (Parker Williams & Hunt Jr., 2002) using AVIRIS data. In this study, the technique was applied using each mangrove species as endmembers.

3.4.1.1 Data reduction and endmember selection for the mangrove species

Dimensionality reduction refers to the process by which the main components attributing to the spectral variance of the data set are identified. The aim is to reduce the information present in hyperspectral imagery so that it can be displayed in a minimized form without any alteration to the original data (Keshava & Mustard, 2002). The procedure used to achieve this was the Minimum Noise Fraction (MNF) implemented in ENVI®. The MNF transformation decomposes the data into the main components contributing most of the spectral variance and also accounts for the noise present in the data (Keshava & Mustard, 2002). The noise is first estimated resulting in a noise covariance matrix, which is then used to decorrelate and rescale the noise in the data. In the transformed data the noise has unit variance and no band-to-band correlation. A PCA is then applied to the noise-whitened data (ENVI, 2001). Two approaches were undertaken to find endmembers representative of each species. For the *A. marina* dominated low closed-forest community the endmember was selected from regions of interest (ROI) corresponding to the two plots for which field data indicated these were monospecific patches of *Avicennia marina*. For the low woodland community the endmembers were selected from the pixel cloud created with MNF bands 1, 8 and 9. The MNF band 9 showed that brighter pixels corresponded to Site 1 where *Aegiceras corniculatum* was dominant in terms of ground cover and projective foliage cover.

3.4.1.2 MTMF of the mangrove species and display

The MF score band and the infeasibility band were used to create a 2-dimensional scatter plot in order to select pixels that matched well with the reference endmember. Pixels of low infeasibility and MF score higher than approximately 0.25 were highlighted. These pixels corresponded to areas where the endmember was recorded as present at a sub-pixel level at a proportion according to the MF score (where 1 = 100 %). The maps were compared to the plots taped in the field for each community and to areas visited in the field that contained these communities. The MTMF results were assessed by correlating the ground-cover measurements taken for each site with the estimated cover of each species at the sub-pixel level. The Pearson correlation coefficient (r^2) was calculated to determine the correlation between the predicted and actual species ground cover. The correlation was applied to the *A. corniculatum* endmember only-the reason being that the *A. marina* endmember resulted in high MF scores and high infeasibility values for some of the low woodland areas making the data unsuitable for the comparisons between actual and predicted species cover.

3.4.2 Supervised classification- Spectral Angle Mapper (SAM)

In the spectral angle mapper (SAM) classification, pixels are considered vectors in n-dimensional space according to their DN values for each band, where the number of dimensions is equal to the number of bands (Kruse *et al.*, 1993).

SAM classifies pixels according to the angular distance between two vectors, the approach ignores vector lengths and is therefore unaffected by illumination effects (Mustard and Sunshine, 1999). Vectors with small angles are considered spectrally similar during the classification and the user must define the minimum spectral angle threshold to which all angles are compared. In this case the angle was set to 0.1 radians for all classes.

Regions of interest (ROI) were created for each community according to the position of their respective plot taped in the field. Additional spectral classes were also created using the information obtained during the endmember selection and field knowledge. A false color composite (RGB:50,33,17) was used to define other spectral classes, with all classes subsequently plotted in 2-to 3-dimension scatter plots using the original image bands. The visible and near infrared bands were used as vegetation features were of greatest interest. Pixels that plotted at the extremities of the spectral clouds were deleted from the class. The maximum, minimum, mean and standard deviation signature of each class were also calculated. These were inspected to ensure that the spectral variance was normal for each class. Supervised classifications were run using the original classes created, which included all 6 communities described in previous sections, and the newly created classes.

3.4.2.1 Accuracy assessment

The accuracy of the resulting images was assessed by calculating confusion matrices that show the level of accuracy of each classified image (Congalton & Green, 1999). Producer's and user's accuracies were calculated for each class, as well as the errors of omission and commission, overall accuracy and kappa coefficients. For each class additional non-biased regions of interest (ROI) were selected and used to calculate the statistics. For the mangrove and saltmarsh classes the regions of interest were defined by field checking carried out on the 20 and 25 November 2002. During field visits a Global Positioning System (GPS) was used to record the coordinates of the areas of interest. For the casuarina forest and littoral forest the ROIs were defined from maps already produced for the area by Chafer (1997) and Carne (1991) (not shown). For the other classes, defined from spectral analysis, false colour composites and scatter plots, the additional ROIs used for the accuracy assessment were defined from the false colour composite. The spectral signatures of these regions were inspected in order to ensure the pixels belonged to the relevant classes. The water classes, such as 'ocean' or 'river', were not included in the accuracy assessment. These classes were not correctly classified by SAM and it was determined that inclusion of the water classes would decrease the overall accuracy of the SAM classification.

4 Results

4.1.1 MTMF (Mixture Tuned Matched Filtering)

The mean spectral reflectance of the *A. marina* and *A. corniculatum* endmembers are shown in Figure 4.1. The spectral reflectance of the *A. marina* endmember is higher in the middle infrared than for the *A. corniculatum* endmember. Spectral reflectance for the *A. corniculatum* endmember is higher in the visible, from the green and red (559 nm to 661 nm) and in the left shoulder of the near infrared plateau from 750 nm to 1100 nm. Both endmembers have high absorbance in the chlorophyll band at approximately 675 nm. Figure 4.2 shows the scatter plot of the MNF bands 1, 8 and 9 and the pixels of *A. corniculatum* endmember that plotted to one of the corners.

The distribution of the *A. marina* endmember is shown in Figure 4.3. Pixels that resulted in low infeasibility values and high MF scores ranging from 0.35 to 1.35 are painted green. Colored pixels on the image represent areas where the *A. marina* endmember has been identified as present. The distribution of the *A. marina* endmember corresponds to Sites 4 and 5 (shown with an arrow) and other areas of the low-intertidal zone closer to the mouth of the estuary (circled) that have been visited and confirmed as being dominated by *A. marina* trees or shrubs. High MF scores and infeasibility values were recorded for some low woodland pixels. These areas were not highlighted since the MF scores are in reality 'false positives' (Boardman, 1998; ENVI, 2001) and do not match correctly with the *A. marina* endmember. The distribution of the *A. corniculatum* endmember is shown in Figure 4.4. The sub-pixel abundance for this species agrees with the distribution of field sites corresponding to the low woodland community. The distribution also extends to the upstream sections, over the low-intertidal zone. Correlation analysis between the actual and predicted ground cover of *A. corniculatum* indicated a high correlation between the predicted and actual abundance of the species (r^2=0.879).

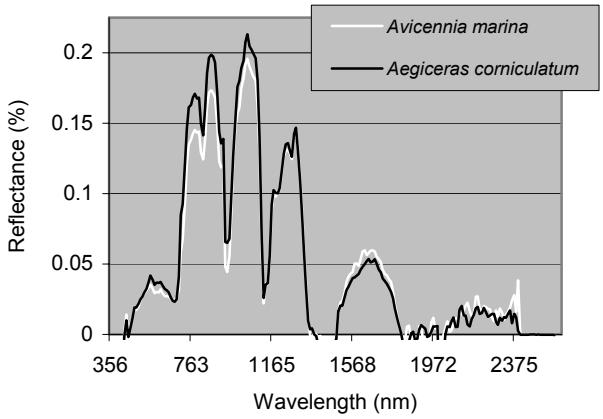

Figure 4.1. Spectral reflectance of the endmembers used in the MTMF of the two mangrove species; *Avicennia marina* (white) and *Aegiceras corniculatum* (black), obtained from the EO-1 Hyperion image subset of the Minnamurra estuary.

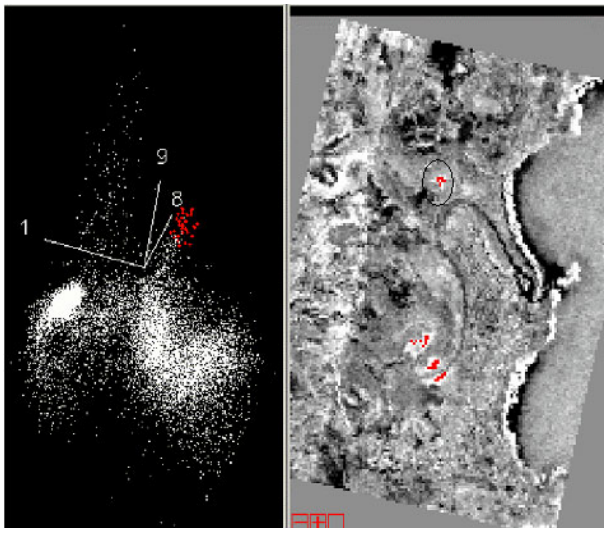

Figure 4.2. Scatter plot of MNF bands 1, 8 and 9 obtained from the EO-1 Hyperion image subset of the Minnamurra estuary (left) and the image subset of the area (right). Position of *Aegiceras corniculatum* endmember in the scatter plot (red pixels) and its spatial distribution in the area (red). *A. corniculatum* pixels corresponding to one of the plots (circled).

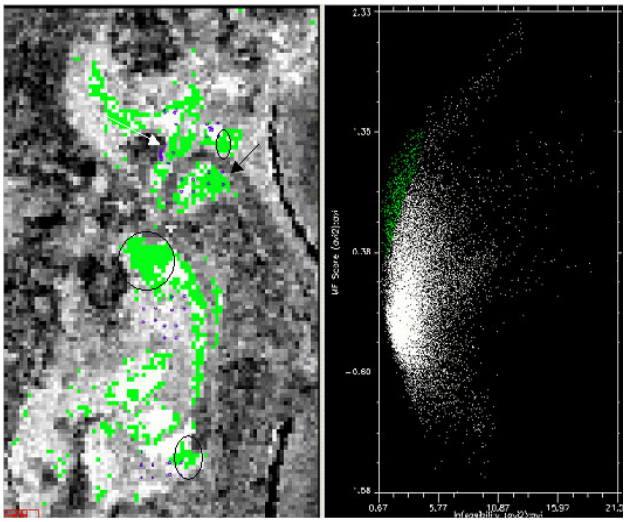

Figure 4.3. Distribution of the *Avicennia marina* endmember (green) obtained from the MTMF applied to the EO-1 Hyperion subset of the Minnamurra estuary (left). The image shows the coordinates of all sites (blue dots), low closed-forest (white and black arrow), and areas confirmed to be composed of *A. marina* (circled). Corresponding pixels in the scatter plot (right), showing high MF (matched filtering) scores and low infeasibility values (green).

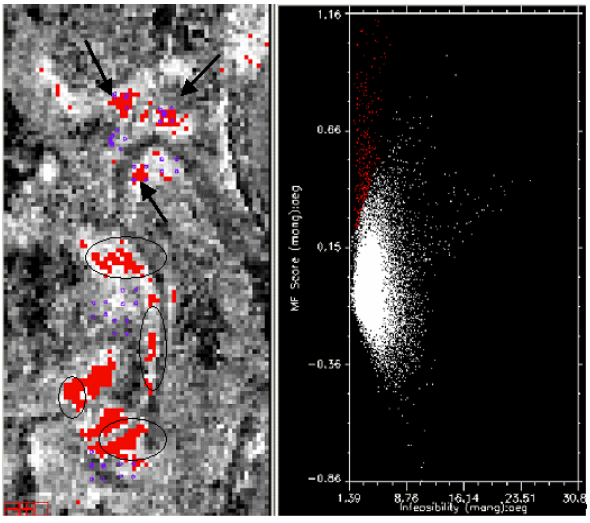

Figure 4.4. Distribution of the *Aegiceras corniculatum* endmember (red) obtained from the MTMF applied to the EO-1 Hyperion subset of the Minnamurra estuary (left). Shows: coordinates of all sites (blue dots), low woodland plots (arrows), and areas confirmed to be composed of *A. corniculatum* (circled). Corresponding pixels in the scatter plot (right), showing high MF (matched filtering) scores and low infeasibility values (red).

4.1.2 Supervised classifications (SAM)

The resulting map from the supervised classification agreed with the distribution of land-cover types at the landscape scale. Major cover classes, such as the urban areas, grasslands and littoral forests, were mapped in accordance to their distribution. In addition, the intertidal vegetation was discriminated well from the rest of the vegetation in the area. Figure 4.5a shows the distribution maps produced for the aggregated saltmarsh and mangrove

classes using the SAM classification and the already created map for the area. Table 4.1 shows the confusion matrix created with the mangrove and saltmarsh classes aggregated.

Table 4.1. Confusion matrix for the distribution map corresponding to Fig 4.5a, produced with the SAM applied to the EO-1 Hyperion subset of the Minnamurra estuary. All aggregated classes.

Overall accuracy = 76.74 % Kappa Coefficient = 0.73											
	Ground Truth (pixels)										
Class	bare ground	dry grass	mangroves	casuarina forest	saltmarsh	littoral forest	urban	green grass	Total	User's (%)	Commission (%)
unclassified	16	2	93	78	27	25	13	2	256		
bare ground	**87**		2				2	1	92	94.57	5.43
dry grass	1	**86**						2	89	96.63	3.37
mangroves			**257**	11	6	1			275	**93.45**	6.55
casuarina forest			20	**113**	2	10			145	**77.93**	22.07
saltmarsh			1	2	**38**				41	**92.68**	7.32
littoral forest			3	5		**90**			98	91.84	8.16
urban	16		4	4	17	1	**301**	1	344	87.5	12.5
green grass		2		1		12		**292**	307	95.11	4.89
Total	120	90	380	214	90	139	316	298	1647		
Producer's (%)	72.5	95.56	**67.63**	**52.8**	**42.22**	64.75	95.25	97.99			
Errors of Omission (%)	27.5	4.44	32.37	47.2	57.78	35.25	4.75	2.01			
Unclassified (%)	13.33	2.22	24.47	36.45	30	17.99	4.11	0.67	15.54		

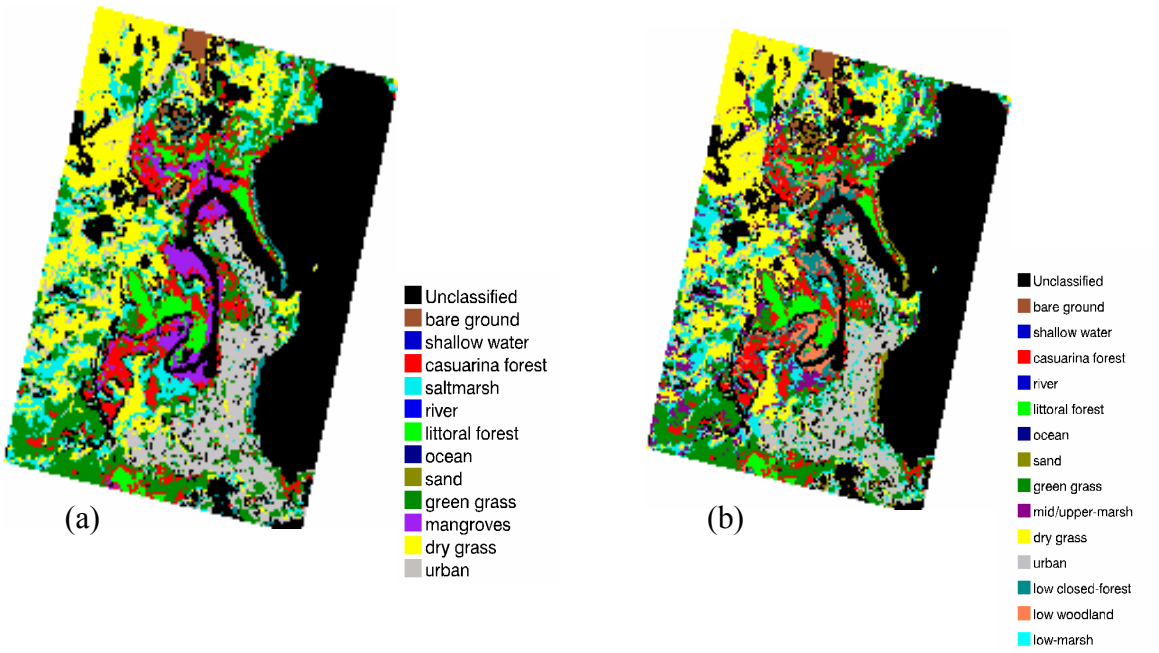

Figure 4.5. Distribution maps resulting from a SAM classification applied to the EO-1 Hyperion image subset of the Minnamurra River Estuary, NSW. (**a**) aggregated mangrove and saltmarsh classes (**b**) not aggregated mangrove and saltmarsh classes. Each image represents an area of 4 km by 5.7 km.

The confusion matrix corresponding to Figure 4.5b (Table 4.2) shows the mangrove class and casuarina forest class were accurately discriminated with producer's accuracies of 62.47 % and 67.29%, respectively. The saltmarsh class recorded lower levels of producer's accuracy of 42.22%. The user's accuracies were higher, approximately 90 % for all three wetland vegetation classes, however, the saltmarsh vegetation was erroneously mapped at high elevations as it was confused with the upland grasses and urban areas. The distribution maps produced by the SAM of the two mangrove classes are shown in Figure 4.5b. The distribution of low closed-forests is restricted to the mouth of the estuary and to the low-intertidal zone, while the distribution of low woodlands is more extensive in the low-intertidal zone upstream and in the upper intertidal zone downstream. The producer's accuracy for the low closed-

forest and the low woodland classes were 57.69 % and 56.67 %, respectively. The confusion occurs mainly between the two mangrove classes (Table 4.2). For example, some pixels corresponding to the low closed-forests were classified as low woodland, while some pixels known to contain mainly *A. corniculatum* shrubs were classified as low closed-forest (Table 4.2). The classifier produced good results, especially considering that around 10 % of the pixels in both classes remained unclassified.

Table 4.2. Confusion matrix corresponding to Figure 4.5b obtained for the SAM classification. Showing the discrimination of the two mangrove communities, low-marsh, mid/upper-marsh and casuarina forest.

Overall Accuracy=66.39 % Kappa Coefficient = 0.61													
	Ground Truth (pixels)												
Class	bare ground	dry grass	low-closed forest	low woodland	low-marsh	mid/upper-marsh	green grass	urban	littoral forest	casuarina forest	Total	User's (%)	Commission (%)
unclassified	50	3	16	11	3	0	3	18	2	2	108		
bare ground	**33**										33	100	0
dry grass	9	**80**						8			97	82.47	17.53
low-closed forest			**60**	44	1	1				40	146	**41.1**	**58.9**
low woodland			24	**85**					3	17	129	**65.89**	**34.11**
low-marsh	2				**4**	26	27	16			75	**5.33**	**94.67**
mid/upper marsh		5			3	**19**	3			1	31	**61.29**	**38.71**
green grass						2	**237**	24	14	20	297	**79.8**	**20.2**
urban	5	2						**250**		1	258	96.9	3.1
littoral forest							6		**85**	10	101	84.16	15.84
casuarina forest			4	10	1		22		35	**123**	195	**63.08**	**36.92**
Total	99	90	104	150	12	48	298	316	139	214	1470		
Producer's accuracy (%)	33.33	88.89	**57.69**	**56.67**	**33.33**	**39.58**	79.53	79.11	61.15	**57.48**			
Errors of Omission (%)	66.67	11.11	**42.31**	**43.33**	**66.67**	**60.42**	20.47	20.89	38.85	**42.52**			
Unclassified (%)	50.51	3.33	**15.38**	**7.33**	**25**	**0**	1.01	5.7	1.44	**0.93**	7.35		

5 Conclusion

The MNF transformation applied to the Hyperion imagery showed that MNF band 9 corresponded with the distribution of *A. corniculatum*, especially in areas of high cover. The MTMF results obtained by using the *A. corniculatum* endmember agreed strongly with the distribution of this species. Its presence was recorded in the three plots and in other areas visited and confirmed (Fig. 4.4). The correlation analysis resulted in high positive correlation between the predicted cover of the *A. corniculatum* endmember and the actual cover measured in the field (r^2=0.879). Similarly the distribution obtained for the *A. marina* endmember showed that the distribution agreed with the two low closed-forest plots and other areas in the low-intertidal zone around the mouth of the estuary (Fig. 4.3), where this species has a high cover and forms extensive monospecific stands.

In mangrove forests, correlations have been found between the projective foliage cover (and leaf area index (LAI)) and the red and near infrared canopy reflectance (Jensen *et al.* 1991; Ramsey & Jensen, 1996; Green *et al.*, 1997), where increases in foliage cover result in increases of near infrared reflectance. However, no correlations have been established between species cover and any of the broad bands used by the most common satellite-borne sensors (Jensen *et al.*, 1991; Ramsey & Jensen, 1996). Previous studies have established that mangrove species could not be discriminated with broad-band satellite sensors because of the low spectral and spatial resolutions (Green *et al.*, 1996; 1998). Therefore, zonation has been mapped according to the structure of the vegetation in each zone (Blasco *et al.*, 1998; Rasolofoharinoro *et al.*, 1998) and the reflectance in the red and near infrared bands. The present study indicates that the improved spectral resolution of Hyperion, which allows for the application of more sophisticated methods of image analysis such as the MTMF, results in a good discrimination of the two mangrove species assessed in this study, despite the apparently low SNR (1:100) of the sensor (Kruse *et al.*, 2001) and 30 m pixels.

6 References

Blasco, F., Saenger, P. & Janodet, E. 1996. Mangroves as indicators of coastal change. *Catena* 27, 167–178.

Blasco, F., Gauquelin, T., Rasolofoharinoro, M., Denis, J., Aizpuru, M. & Caldairou V. 1998. Recent advances in mangrove studies using remote sensing data. *Marine and Freshwater Research* 49, 287–296.

Boardman, J.W. 1998. Leveraging the high dimensionality of AVIRIS data for improved sub-pixel target unmixing and rejection of false positives: Mixture Tuned Matched Filtering. *Summaries of the Seventh JPL Airborne Geoscience Workshop, JPL Publication 97-1* (pp. 55–56) Pasadena, CA: NASA Jet Propulsion Laboratory.

Carne, J. 1991. Landform vegetation relationships in the Minnamurra estuary, NSW, Monograph Series, No. 6, Department of Geography and Oceanography, University College, Australian Defense Force Academy, Canberra.

Chafer, C.J. 1997. *Biodiversity of Wetlands in the Illawarra Catchment: An inventory*. Illawarra Management Committee, Wollongong.

Clark, R.N. 1999. Spectroscopy of rocks and minerals, and principles of spectroscopy. *In* Andrew N.R. ed. *Remote Sensing for the Earth Sciences: Manual of Remote Sensing, 3 ed., Vol. 3* pp 3–58. John Wiley & Sons, Inc.

Congalton, R.G. & Green K. 1999. *Assessing the Accuracy of Remotely Sensed Data: Principles and Practices.* Lewis Publishers, Washington D.C.

Curran, P. J. 1994. Imaging spectrometry. *Progress in Physical Geography* 18: 247–266.

Dehaan, R.L. & Taylor G.R. 2002. Field-derived spectra of salinized soils and vegetation as indicators of irrigation-induced soil salinization. *Remote Sensing of Environment* 80, 406–417.

ENVI. 2001. ENVI (Environment for Visualizing Images) User's Guide: Images to Information. Research Systems, Inc., Boulder CO.

Environment Australia 2001. *A Directory of Important Wetlands in Australia*. 3rd Edition. Environment Australia, Canberra.

Finlayson, C.M., Davison N.C., Spiers A.G. & Stevenson N.J. 1999. Global wetland inventory-current status and future priorities. *Marine and Freshwater Research* 50, 717–727.

Green, E.P., Mumby P.J., Edwards A.J., Clark C.D. & Ellis A.C. 1997. Estimating leaf area index of mangroves from satellite data. *Aquatic Botany* 58, 11–19.

Green, E.P., Clark C.D., Mumby P.J., Edwards A.J. & Ellis A. 1998. Remote sensing techniques for mangrove mapping. *International Journal of Remote Sensing* 19, 935–956.

Gross, M.F., Hardinsky M.A. & Klemas V. 1989. Applications to coastal wetlands vegetation. *In* Asrar G. ed. *Theory and Application of Optical Remote Sensing*, pp. 474–490. John Wiley and Sons, New York.

Holmgren, P. & Thuresson T. 1998. Satellite remote sensing for forestry planning-a review. *Scandinavian Journal of Forest Research* 13, 90–110.

Jensen, J.R., Lin H., Yang X., Ramsey III E., Davis B. A & Thoemke C.W. 1991. The measurement of mangrove characteristics in Southwest Florida using SPOT multispectral data. *Geocarto International- A Multidisciplinary Journal of Remote Sensing* 6, 13–21.

Jupp, D.L.B., Datt B., Lovell J., Campbell S. & King E. 2002. *Discussions around Hyperion data: background notes for the Hyperion data users workshop.* CSIRO Office of Space Science & Applications, Earth Observation Center, Canberra. (unpublished).

Keshava, N. & Mustard J.F. 2002. Spectral unmixing. *IEEE Signal Processing Magazine* 19, 44–57.

Klemas, V.V. 2001. Remote sensing of landscape-level coastal environmental indicators. *Environmental Management* 27 (1), 47–57.

Kruse, F.A., Lefkoff A.B. & Dietz J.B. 1993. The Spectral Image Processing System (SIPS)- Interactive visualization and analysis of imager spectrometer data. *Remote Sensing of Environment* 44, 145–163.

Kruse, F.A., Boardman J.W. & Huntington J.H. 2001. Progress report: geologic validation of EO-1 Hyperion using AVIRIS. *Proceedings of the Tenth JPL Airborne Geoscience Workshop, JPL Publication 02-1*. http://popo.jpl.nasa.gov/docs/workshops/01_docs/2001Kruse_web.pdf

Küchler, A.W. 1988. Basic considerations: The nature of vegetation. *In* Küchler A.W. & Zonneveld I.S. eds. *Vegetation mapping* pp. 13–23. Klewer Academic Publishers, Dordrecht.

Lewis, M.M. 1999. *Discriminating Arid Vegetation Composition with Multispectral and High Spectral Resolution Imagery.* PhD thesis, University of New South Wales (unpublished).

McDonald, R.C., Isbell R.F., Speight J.G., Walker J. & Hopkins M.S. 1984. *Australian Soil and Land Survey: Field Handbook*. Inkata Press, Melbourne.

Muller, E. 1997. Mapping Riparian Vegetation along rivers: old concepts and new methods. *Aquatic Biology* 58: 411–437.

Mumby, P. J., Green, E. P., Edwards, A. J. Clark, C. D. 1999. The cost-effectiveness of remote sensing for tropical coastal resources assessment and management, *Journal of Environmental Management* 55: 157–166.

Mustard, J.F. & Sunshine J.M. 1999. Spectral analysis for Earth science: investigations using remote sensing data. *In* Andrew N.R. ed. *Remote Sensing for the Earth Sciences: Manual of Remote Sensing, 3 ed., Vol. 3* pp 251–306. John Wiley & Sons, Inc.

Parker Williams A. & Hunt Jr. E.R. 2002. Estimation of leafy spurge cover from hyperspectral imagery using mixture tuned matched filtering. *Remote Sensing of Environment* 82, 446–456.

Phinn S., Hess L. & Finalyson C. M. 1999. An assessment of the usefulness of remote sensing for coastal wetland inventory and monitoring in Australia. *In* Finlayson C.M. & Spiers A.G. eds. *Techniques for enhanced wetland inventory and monitoring.* Supervising Scientist Environment Australia, Canberra.

Pinzon J. E., Ustin S.L., Castaneda C.M. & Smith M.O. 1998. Investigation of leaf biochemistry by Hierarchical Foreground/Background Analysis. *IEEE Transactions on Geoscience and Remote Sensing* 36, 1913–1927.

Ramsey III E.W. & Jensen J.R. 1996. Remote sensing of mangrove wetlands: relating canopy spectra to site-specific data. *Photogrammetric Engineering and Remote Sensing* 62, 939-948.

Rasolofoharinoro M., Blasco F., Bellan M.F., Aizpuru M., Gauquelin T. & Denis J. 1998. A remote sensing based methodology for mangrove studies in Madagascar. *International Journal of Remote Sensing* 19, 1873–1886.

Richard J.A. & Jia X. 1999. *Remote Sensing Digital Image Analysis: An Introduction.* 3rd Edition. Springer, Berlin.

Rougharden J., Running S.W. & Matson P.A. 1991. What does remote sensing do for ecology? *Ecology* 72, 1918–1922.

Saenger P., Specht M.M., Specht R.L. & Chapman, V.J. 1977. Mangal and coastal salt-marsh communities in Australasia. *In* VJ Chapman ed. *Wet Coastal Ecosystems* pp.293–345. Elsevier, Amsterdam.

Serrano L., Penuelas J. & Ustin S.L. 2002. Remote sensing of nitrogen and lignin in Mediterranean vegetation from AVIRIS data: Decomposing biochemical from structural signals. *Remote Sensing of Environment* 81, 355–364.

Ustin S.L., Wessman C.A., Curtiss B., Kasischke E., Way J. & Vanderbilt V.C. 1991. Opportunities for using the EOS imaging spectrometers and synthetic aperture Radar in ecological models. *Ecology* 72, 1934–1945.

Vane G. & Goetz A.F.H. 1993. Terrestrial imaging spectrometry: current status, future trends. *Remote Sensing of Environment* 44, 117–126.

Zhang M., Pinzon J., Ustin S.L. & Rejmankova E. 1996. Differentiating salt marsh species using Foreground/Background analysis. *Proceedings of the ERIM Second International Airborne Remote Sensing Conference and Exhibition*, San Francisco. 1, 83–91.